

# Learning to Recognize Patch-Wise Consistency for Deepfake Detection

Tianchen Zhao\* Xiang Xu Mingze Xu Hui Ding Yuanjun Xiong Wei Xia  
Amazon/AWS AI

ericolon@umich.edu, {xiangx, xumingze, huidin, yuanjx, wxia}@amazon.com

## Abstract

We propose to detect Deepfake generated by face manipulation based on one of their fundamental features: images are blended by patches from multiple sources, carrying distinct and persistent source features. In particular, we propose a novel representation learning approach for this task, called patch-wise consistency learning (PCL). It learns by measuring the consistency of image source features, resulting to representation with good interpretability and robustness to multiple forgery methods. We develop an inconsistency image generator (I2G) to generate training data for PCL and boost its robustness. We evaluate our approach on seven popular Deepfake detection datasets. Our model achieves superior detection accuracy and generalizes well to unseen generation methods. On average, our model outperforms the state-of-the-art in terms of AUC by 2% and 8% in the in- and cross-dataset evaluation, respectively.

## 1. Introduction

Face manipulation [43] has been emerging as a prominent stream of deep face forgery. It replaces the identity or expression of a target subject with that of another subject, by stitching image patches from different sources together. Extensive work has been done to detect manipulated facial images and videos [63, 28, 40, 55, 50, 7, 25, 52, 24, 8], with the attempt to spot various faking cues, such as eye blinking [28], face warping [29], blending boundaries [25], fake prototypes [52], etc. However, most of the work focuses on implicitly or explicitly capturing holistic representations to identify suspicious artifacts from specific synthetic methods. As a result, the learned models are able to detect artifacts seen during their training, but have trouble keeping up with unseen Deepfake generation methods and more advanced blending techniques.

We tackle the above issue by utilizing the fundamental feature of Deepfake generated by face manipulation: blending images from multiple sources. Images from different

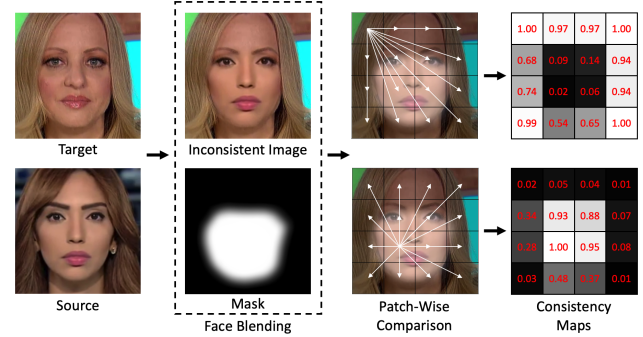


Figure 1: An overview of our patch-wise consistency learning. An “self-inconsistent” image is generated by stitching the target and source faces, where the mask indicates the region of modification and separates the patches into two groups. For each patch, we compute its source features consistencies with the rest, and their corresponding consistency scores are shown on the right.

sources carry *distinctive* source features, such as in-camera features (e.g., PRNU noise [32], specifications [17]), out-camera features (e.g., JPEG compression patterns [3], compression rates, frame rates), and forgery features (e.g., copy-paste artifacts [2], blending artifacts [25], GAN fingerprints [62]). And these cues are still preserved after being stitched into Deepfake images, even with state-of-the-art generation and blending methods. Therefore, Deepfake images are poised to contain different source features in different locations, whereas the source features of a pristine image must be *self-consistent* across all of its patches despite the variation of their semantic contents [17]. By building representation models that separate the different source features in different image patches, we may be able to effectively detect manipulated face images, even for those from unseen generation techniques.

In this paper, we explore this paradigm of *detecting Deepfake by source features consistency*. We propose a novel representation learning method, called Patch-Wise Consistency Learning (PCL), and present experimental results showing that predicting the self-consistency of source features indeed improves the performance of Deepfake detection. In particular, classification is built on the learned consistency features and the consistency map is predicted

\*Currently at University of Michigan, Ann Arbor. The work was conducted during internship at AWS.

to provide an intuitive visual explanation of the manipulated regions. Fig. 1 illustrates an example of our consistency learning pipeline. We split the input frame into small patches and cluster them into groups according to their pairwise similarity score of source features. A non-linear classifier is built upon the learned similarity representation for binary Deepfake prediction.

Learning with PCL requires patch-level annotation of the manipulated regions which is not widely available. We develop the Inconsistency Image Generator (I2G), which synthesizes “inconsistent” samples by face manipulation using the pristine images along with random “forgery masks” and thus also produces ground truth for PCL supervision. Different from other data generators [17, 29], in I2G, we introduce random blending and strong data augmentation to enhance the robustness of PCL learned representation against attempts to hide source features in Deepfake.

The contributions of this paper are three-fold. First, we introduce Patch-Wise Consistency Learning (PCL) to Deepfake detection, which is more robust to unseen generation methods. Second, we propose an end-to-end learning architecture to realize PCL in practice, which can work with various backbones as a plugin module and produces interpretable visualization. Third, we evaluate the performance of our model on seven public-available datasets. To evaluate the generalization ability, we also conduct the cross-dataset experiment, where we train and test PCL on separate datasets with different generation methods. Experimental results show that, on average, our approach outperforms the state-of-the-art in terms of AUC by 2% and 8% in the in- and cross-dataset evaluation, respectively. We believe that our work provides a comprehensive benchmark for future work on Deepfake detection.

## 2. Related Work

**Deepfake Generation.** In general, there are four common types of Deepfake [51]: whole image synthesis, modification of facial attribute or expression, and face identity swap. The 3D models [48], AutoEncoders [47, 53], or Generative Adversarial Networks [19, 20, 31, 6] are used to generate the image and blend it back to the original images.

**Deepfake Detection.** To detect the whole image synthesis, recent research [62, 39, 16, 56] observes that generated images contain specific cues that can be easily detected, and the trained models have exhibited good generalization ability across synthesis methods. To support the research on detecting the other types of face manipulations, several Deepfake datasets are released [61, 22, 45, 12, 30, 10, 18, 64] and countermeasures have been introduced. *FakeSpotter* [55] is proposed with a layer-wise neuron behavior for fake face detection. *Tolosana et al.* [50] split the facial image into pieces and make binary predictions on these local re-

gions. *Kumar et al.* [24] train a triplet network with positive and negative samples. Recurrent neural networks [46] and various types of 3D ConvNets [8] are utilized to detect the manipulation artifacts across the video frames. However, binary classifiers are criticized for their interpretability, and several localization methods are introduced through either multi-task learning [40] or attention-based mechanisms [7]. To improve the generalization ability, *DSP-FWA* [29] and *Face X-ray* [25] also make their own data generation pipeline and the latter focuses on predicting the blending boundaries in fake video frames. Our approach also lies in this line but has several main differences. First, from a methodology perspective, our approach focuses on learning similarity representations by measuring local patch consistency for patch-wise consistency recognition rather than spotting face wrapping or blending artifacts; Second, from a network design perspective, our approach is more simple, which can use any common network as the backbone. The designed inconsistency predictor only contains a few parameters and can serve as a plugin module.

**Consistency Learning.** The concept of inconsistency has been studied in the image forensic literature [37], where image patches are fed as inputs to the model to predict the similarity scores [37, 36, 17, 35, 63, 4]. *Zhou et al.* [63] propose a two-stream network to detect both tampered faces and low-level inconsistencies among image patches, but the training is not end-to-end and requires additional steganalysis feature extraction. *Huh et al.* [17] use a Siamese network to predict the image metadata inconsistency on the local patches cropped from the different images. We introduce consistency learning to Deepfake detection and propose a practical end-to-end consistency learning architecture.

## 3. Our Approach

Given an input video frame that contains one or more faces, our goal is to detect if the identity or expression of a target subject is swapped with that of a source subject. Observing that Deepfake images are blended by patches from multiple sources with distinct source features, we explore to learn effective and robust representations for Deepfake detection by measuring the consistency of image source features. More specifically, we propose a multi-task learning architecture, as shown in Fig. 2. The consistency branch is optimized to predict a consistency map for each image patch, indicating if its source features are consistent with all others. We integrate the consistency maps together as a visualization heatmap, which ideally identifies the manipulated regions and provides a better interpretation for human analysis. The classification branch is applied to the learned features and outputs binary scores for forgery detection.

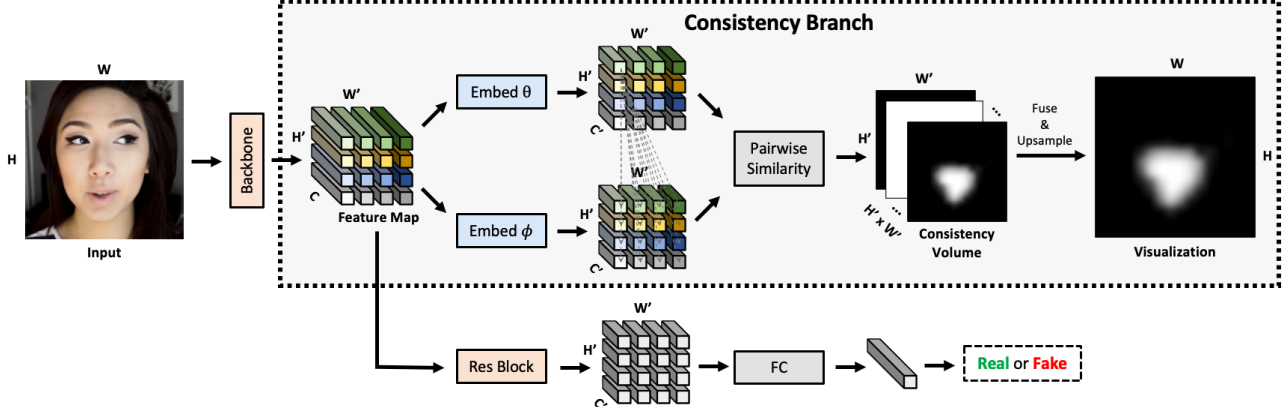


Figure 2: *Visualization of PCL architecture*. The consistency branch focuses on measuring the consistency of image patches according to their source features, and outputs a visualization map that indicates the manipulated region. A classification branch is applied after the learned feature map and predicts the binary score for Deepfake detection.

### 3.1. Patch-Wise Consistency Learning (PCL)

The **consistency branch** computes the pairwise similarity scores of all possible pairs of local patches in an image and predicts a 4D consistency volume  $\hat{V}$ . Given a pre-processed video frame  $X$  of size  $H \times W \times 3$  as input, we first feed it into the backbone and extract the feature  $F$  of size  $H' \times W' \times C$  from an intermediate convolution layer, where  $H'$ ,  $W'$ , and  $C$  are height, width, and channel size, respectively. For each patch  $\mathcal{P}_{h,w}$  in the extracted feature map, we compare it against all the rest to measure their feature similarities, and obtain a 2D consistency map  $\hat{M}^{\mathcal{P}_{h,w}}$  of size  $H' \times W'$  of consistency scores in the range of  $[0, 1]$ , where the superscript indicates the position of the base patch. To be specific, for any pair of patches  $\mathcal{P}_i$  and  $\mathcal{P}_j$ , we compute their dot-product similarity [57] using their extracted feature vector  $f_i$  and  $f_j$ , both of size  $C$ , to estimate their consistency score:

$$s(f_i, f_j) = \sigma \left( \frac{\theta(f_i)\phi(f_j)}{\sqrt{C'}} \right), \quad (1)$$

where  $\theta$  and  $\phi$  are the embedding functions, realized by  $1 \times 1$  convolutions,  $C'$  is the embedding dimension, and  $\sigma$  is the Sigmoid function. We iterate this process over all patches  $\{\mathcal{P}_{h,w} | 1 \leq h \leq H', 1 \leq w \leq W'\}$  in the extracted feature map, and finally get the 4D consistency volume  $\hat{V}$  of size  $H' \times W' \times H' \times W'$ . To easier interpret and provide visualization clues about the region of modification, we fuse the 4D consistency volume  $\hat{V}$  over all patches and generate a 2D global heatmap  $\hat{M}$  of size  $H' \times W'$ . We up-sample  $\hat{M}$  to  $\hat{M}$  of size  $H \times W$  to match the input size for better visualization, as shown in Fig. 5.

The **optimization of consistency branch** requires the 4D “ground truth” consistency volume  $\mathbf{V}$ . Given the mask  $\mathcal{M}$  of size  $H \times W$  indicating the manipulated region of input

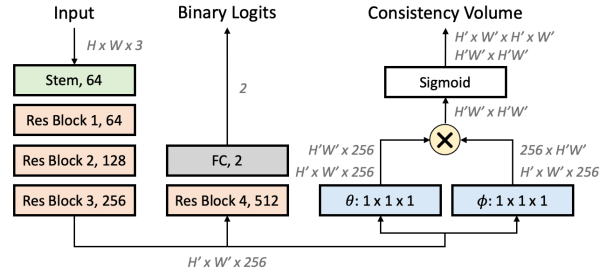


Figure 3: *An example of PCL architecture*, where ResNet-34 is adopted as backbone. The features are shown as the shape of their tensors, and proper reshaping is performed.  $\otimes$  denotes matrix multiplication, and  $\theta$  and  $\phi$  are two  $1 \times 1 \times 1$  convolutions.

$X$ , we first create its coarse version  $\mathcal{M}$  matching the size of  $H' \times W'$  through bi-linear down-sampling. We obtain the ground truth 2D consistency map  $M^{\mathcal{P}_{h,w}}$  for the  $(h, w)$ -th patch by computing the element-wise difference between its own value  $\mathcal{M}_{h,w}$  and all others,

$$M^{\mathcal{P}_{h,w}} = 1 - |\mathcal{M}_{h,w} - \mathcal{M}|, \quad (2)$$

where  $\mathcal{M}_{h,w}$  is the scalar value in position  $(h, w)$ , and  $M^{\mathcal{P}_{h,w}}$  is in size of  $H' \times W'$ . For each entry of  $M^{\mathcal{P}_{h,w}}$ , a value close to 1 denotes the two patches are consistent, and close to 0 otherwise. To obtain the ground truth 4D global map  $\mathbf{V}$ , we compute  $M^{\mathcal{P}_{h,w}}$  for all patches. Note that  $\mathbf{V}$  of a pristine image should be  $\mathbf{1}$ , a 4D volume in which all values are equal or close to one.

We use the binary cross-entropy (BCE) loss to supervise the consistency prediction over the 4D consistency volume  $\hat{V}$ , and more formally,

$$\mathcal{L}_{pcl} = \frac{1}{N} \sum_{h,w,h',w'} \text{BCE}(\mathbf{V}_{h,w,h',w'}, \hat{\mathbf{V}}_{h,w,h',w'}), \quad (3)$$

where  $h$  and  $h' \in [1, H']$ ,  $w$  and  $w' \in [1, W']$ , and  $N$  equals to  $H' \times W' \times H' \times W'$ .

The consistency branch learns the representations that cluster image patches into groups according to their source features, which by our claim could significantly benefit the Deepfake detection in both effectiveness and robustness. Nevertheless, these features cannot directly make inferences for detection purposes.

**The classification branch** is applied after the learned feature map to predict whether the input is real or fake. More specifically, the intermediate extracted feature  $F$  is fed into another convolution operation. A global average pooling and fully-connected layer are built after that as the classifier, which outputs the probability score for the input of being fake or real. We use the two-class cross-entropy (CE) loss  $\mathcal{L}_{cls}$  to supervise the training in the classification branch.

Fig. 3 illustrates an example of the PCL architecture, and the overall loss function of our model is defined as follows:

$$\mathcal{L} = \lambda \mathcal{L}_{pcl} + \mathcal{L}_{cls}, \quad (4)$$

with hyper-parameter  $\lambda$ . The ablation study in Section 4.5 suggests that a choice of large  $\lambda$  value significantly improves the performance. This observation demonstrates that the representations learned from the consistency branch play a dominant role in the success.

### 3.2. Inconsistency Image Generator (I2G)

Training PCL requires data with patch-level annotation of the manipulated regions, which is not always available in existing datasets. To provide this training data, we propose *Inconsistency Image Generator (I2G)* to generate “self-inconsistent” images from the pristine ones, along with the ground truth masks  $\mathcal{M}$  discussed in Section 3.1. Similar self-supervised approaches [29, 25, 38, 10] have been studied in other tasks or methods for Deepfake detection.

I2G particularly addresses several challenges to fit PCL better. **First**, because face images have some strong structural bias, the localized pair sampling scheme in PCL could lead to overfitting to face region information instead of learning to distinguish source features. I2G uses elastic deformation [44] to remove the bias in pairs-sampling for the loss computation in Eq. 3. In practice, we found that this step is particularly crucial in ensuring that the learned representation can distinguish source features, upon which an effective classifier can be learned that generalizes well. **Second**, because attackers will intentionally try to remove source features to make Deepfake images more realistic, PCL needs to make use of source features that are not vulnerable to these approaches. I2G randomly selects one from an exhaustive set of blending methods in data generation so the representation learned by PCL can be robust to source feature removal attempts. **Third**, we expect the learned representation to generalize to a wide range of sources, even unseen during training. I2G adds image augmentation to the

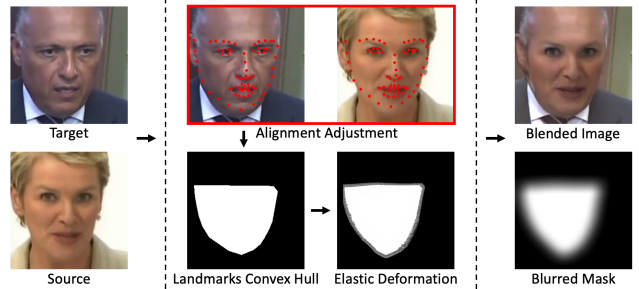


Figure 4: Illustration of the workflow of I2G. For each source and target frame pair, a morphed mask is generated by taking a convex hull of the landmarks followed by elastic deformation and Gaussian blur. The masked region of the target image is replaced by that of the source with blending techniques [42, 38].

generation process to achieve this goal. The augmentation methods include JPEG compression, Gaussian noise/blur, brightness contrast, random erasing, and color jittering.

---

#### Algorithm 1 Inconsistency Image Generator (I2G)

---

**Input:** Target video frame  $X^t$  of size  $(H, W, 3)$ .

**Output:** Generated video frame  $X^g$  and mask  $\mathcal{M}$ .

**Landmark Detector**  $\mathcal{K} : \mathbb{R}^{H \times W \times 3} \rightarrow \mathbb{R}^{68 \times 2}$ .

- 1: Get the video frame  $X^t$  and its landmarks  $\mathcal{K}(X^t)$ .
- 2: Find a random source frame  $X^s$  of different ID, which satisfies  $\|\mathcal{K}(X^t) - \mathcal{K}(X^s)\|_2 < \epsilon$  for threshold  $\epsilon > 0$ .
- 3: Align  $X^s$  to  $X^t$  using landmarks.
- 4: Compute convex hull  $\mathcal{H}$  of  $\mathcal{K}(X^t)$ .
- 5: Get mask  $\mathcal{M}$  by elastic deforming and blurring  $\mathcal{H}$ .
- 6: Get  $X^g$  by blending  $X^t$  with  $X^s$  with  $\mathcal{M}$ .

---

The workflow of I2G is summarized in Alg. 1 and illustrated in Fig. 4. Given a target video frame  $X^t$ , we take its 68-point facial landmarks and retrieve another frame from different videos with different identities. We make sure that the faces in these two frames have similar landmarks measured in  $\ell_2$  norm. For a pair of images, we first align their faces with the pre-computed landmarks and then detect the facial region by taking the convex hull of the landmarks. Elastic deformation [44] is also employed to morph the convex hull: we generate the smooth deformations using random displacement vectors sampled from a Gaussian distribution with a standard deviation of 6 to 12 pixels on a coarse 4 by 4 grid, and compute per-pixel displacements using bicubic interpolation. The deformed mask is further blurred by a Gaussian kernel of size 16. Finally, the facial region of the source frame within the mask is stitched to the target frame using various blending methods [42, 38]. I2G outputs a forged video frame and the corresponding mask  $\mathcal{M}$ .

I2G could also be utilized as a part of the data augmentation for Deepfake detection. It has a low computational cost and can be used for online data generation on CPU during training. For each epoch, the source video frame that sat-

isfies the condition (Alg. 1 line 2) is randomly chosen to increase the amount and diversity of the dataset.

## 4. Experiments

We evaluated the performance of our approach (PCL + I2G) against multiple state-of-the-art methods on seven publicly-available datasets. First, we showed that our model is able to achieve convincing performance under the in-dataset setting, where training and testing are conducted on the same dataset. To demonstrate that PCL has superior generalization ability, we conducted cross-dataset evaluation by training the model with only I2G-augmented real videos and testing on unseen datasets. The ablation studies explored the contribution of each component in our model, such as the effect of PCL and I2G.

### 4.1. Implementation Details

**Pre-processing.** For each raw video frame, face crops are detected and tracked by using [26] and landmarks are detected by public toolbox [5]. We normalize all face crops with ImageNet mean [0.485, 0.456, 0.406] and standard deviation [0.229, 0.224, 0.225], and resize them to  $256 \times 256$ . We also use standard data augmentations, including flipping, rotation, JPEG compression, and Gaussian noise/blur.

**Network Architecture.** We adopt ResNet-34 [15] with an extra  $3 \times 3$  max pooling operation after the `conv1` layer as backbone and initialized with pretrained weights on ImageNet [9]. Given a pre-processed video frame  $X$  of size  $H \times W \times 3$ , we first feed it into the backbone and extract the features  $F$  after the `conv3` layer of size  $H' \times W' \times 256$ , where  $H' = H/16$  and  $W' = W/16$ . Here each patch corresponds to a  $16 \times 16$  region in the original image.

**Training.** For each epoch, we randomly sample 32 frames from every video, and the total number of training samples from  $K$  videos is  $32 \times K$ . The model is trained for 150 epochs using Adam optimizer [21] with batch size 128, betas 0.9 and 0.999, and epsilon  $10^{-8}$ . The learning rate is linearly increased from 0 to  $5 \times 10^{-5}$  in the first quarter of the training iterations and is decayed to zero in the last quarter. The hyper-parameter  $\lambda$  is set to be 10 by default.

### 4.2. Settings

**Training Data.** Each of our training samples is of the form  $(X, \mathbf{V}, y)$ , where  $X$  is the input video frame,  $\mathbf{V}$  is the ground truth 4D consistency volume, and  $y$  is the binary label. For a real frame,  $\mathbf{V}$  is a 4D tensor of ones, indicating the image is self-consistent, and  $y$  is zero. There are two types of forged samples in our settings. The first type is the Deepfake video frame from the existing Deepfake datasets, for which we find the corresponding real video frame and compute the structural dissimilarity (DSSIM) [59] between them. The mask  $\mathcal{M}$  is then generated by taking a Gaussian blur of

DSSIM followed by thresholding.  $\mathbf{V}$  is computed from  $\mathcal{M}$  by Eq. 2 and  $y$  is one. The second type is the fake image **augmented by I2G** on real images, where  $\mathbf{V}$  is computed with the mask from I2G and  $y$  is one. By training with I2G-augmented datasets, whenever a real data  $(X^t, 1, 0)$  is sampled during the training, there is a 50% chance that it is dynamically transformed by I2G into a fake data  $(X^g, \mathbf{V}, 1)$  where  $X^g$  and  $\mathcal{M}$  are the outputs of I2G as described in Alg. 1 and  $\mathbf{V}$  is computed with  $\mathcal{M}$  by Eq. 2. A proper strategy is to balance the total number of real and fake data when both types of forgeries are involved in the training. Moreover, we observe that the performance of our model is not sensitive to the exact real and fake ratio in the train set, as long as it is not extremely imbalanced.

More specifically, in the **in-dataset experiments**, our train set includes both the pristine and Deepfake videos from the train split of the dataset (to be evaluated). Unless otherwise noted, we also utilize the fake samples augmented by I2G as data augmentation. In the **cross-dataset experiments**, we follow prior work [25] and train with *only real videos* from the raw version of FaceForensics++ (FF++) [45], augmented by I2G.

**Test Data.** **FaceForensics++** (FF++) [45] is by far the most popular dataset in the Deepfake detection research community, with plentiful benchmark results. The raw version of its test set contains 700 videos, including 140 pristine videos and 560 manipulated counterparts from 4 different algorithms, which are Deepfakes (DF) [13], Face2Face (F2F) [48], FaceSwap (FS) [23] and NeuralTextures (NT) [49], respectively. **DeepfakeDetection** (DFD) [12] dataset is released by Google & JigSaw incorporated with the FaceForensics++ team, supporting the Deepfake detection research. **Celeb-DF-v1** (CD1) & **-v2** (CD2) [30] are datasets consisting of high-quality Deepfake celebrity videos using advanced synthesis process. **Deepfake detection Challenge** (DFDC) [10] public test set is a large-scale dataset released for the Deepfake Detection Challenge, and **DFDC Preview** (DFDC-P) [11] is its preliminary version. We observe that both DFDC and DFDC-P contain many extremely low-quality videos, which make them exceptionally challenging. **DeeperForensics-1.0** (DFR) [18] is a recently released dataset, which modifies the pristine videos in FF++ with new face IDs and more advanced techniques. More detailed statistics for test sets is summarized in the Appendix.

**Evaluation Metrics.** We report the Deepfake detection results with the most commonly used metrics in the literature, including **area under the ROC curve (AUC)** and **Average precision (AP)**. A higher AUC or AP value indicates better performance. To provide a comprehensive benchmark for future work, we report our performance on all datasets in terms of AUC, AP, as well as **Equal Error Rate (EER)**

Method	Backbone	Train Set	Test Set (AUC (%))				
			DF	F2F	FS	NT	FF++
MIL [58]	Xception	FF++	99.51	98.59	94.86	97.96	97.73
Fakespotter [55]	ResNet-50	FF++, CD2, DFDC	-	-	-	-	98.50
XN-avg [45]	Xception	FF++	99.38	99.53	99.36	97.29	98.89
Face X-ray [25]	HRNet	FF++	99.12	99.31	99.09	99.27	99.20
S-MIL-T [27]	Xception	FF++	99.84	99.34	99.61	98.85	99.41
PCL + I2G	ResNet-34	FF++	<b>100.00</b>	<b>99.57</b>	<b>100.00</b>	<b>99.58</b>	<b>99.79</b>

Table 1: *In-dataset evaluation results on FF++*. Our method performs better on all manipulation types with fewer network parameters.

Method	Backbone	Train Set	Test Set (AUC (%))	
			CD2	CD2
Fakespotter [55]	ResNet-50	CD2	66.80	
Tolosana <i>et al.</i> [50]	Xception	CD2	83.60	
S-MIL-T [27]	Xception	CD2	98.84	
PCL + I2G	ResNet-34	CD2	<b>99.98</b>	

Table 2: *In-dataset evaluation results on CD2*. We achieve saturated performance in terms of AUC.

Method	Backbone	Train Set	Test Set (AUC (%))	
			DFDC-P	DFDC-P
Tolosana <i>et al.</i> [50]	Xception	DFDC-P	91.10	
S-MIL-T [27]	Xception	DFDC-P	85.11	
PCL + I2G	ResNet-34	DFDC-P	<b>94.38</b>	

Table 3: *In-dataset evaluation results on DFDC-P*. Our method improves the best existing result by 3.28% in terms of AUC.

in the Appendix. Unless otherwise noted, the evaluation results in the experiments are at video-level, computed by averaging the classification scores of the video frames.

### 4.3. In-Dataset Evaluation

In-dataset evaluation is abundantly adopted in the literature, where the focus is on specialization but not generalization. To compare against the existing work, we consider three of the most popular datasets, which are FF++, CD2, and DFDC-P. Given a dataset, our model is trained on both real and Deepfake data from train split, and performance is evaluated with the corresponding test set.

The results for FF++, CD2, DFDC-P are shown in Table 1, Table 2, Table 3, respectively. In particular, our models achieve the state-of-the-art with almost perfect performance on CD2 (99.98%) and all four manipulations of FF++ (100.00% on DF, 99.57% on F2F, 100.00% FS, 99.58% on NT, respectively), surpassing all existing work. For DFDC-P, our model outperforms the state-of-the-art result by 3.28% in terms of AUC score. Note that the results reported for DFDC-P are comparably lower, due to the fact that a non-negligible portion of the dataset is of extremely low quality, *e.g.*, human faces in some videos are hardly recognizable. In addition to video-level evaluation, we also compare with prior work in terms of frame-level AUC on

CD2, and outperform the state-of-the-art [33] by 8%. (see Appendix for more details).

### 4.4. Cross-Dataset Evaluation

The generalization of Deepfake detection is a serious concern even for large-scale training. It is reported that the ranking of top-performing models changes significantly from DFDC public test set to private one [14]. Whether or not a method that achieves good results on its own test set can still perform well on other benchmarks remains unclear.

Table 4 presents the cross-dataset evaluation results on FF++ and DFD datasets, where we only used the real videos of FF++ for training. The performance of our model is on par with Face X-ray [25] on FF++, achieving convincing results with more than 99.00% in terms of AUC. Interestingly, the performance gap between our model and Face X-ray [25] is much larger (99.07% vs. 93.47%) when evaluated on DFD. It is possible that the test data of FF++ is highly correlated with its training data, since they are very likely to be collected from the same source, whereas the correlation disappears in DFD. The results demonstrate that predicting the source features consistency can effectively generalize across different source cues, without overfitting to any spurious correlation among data from the same generation method.

We further evaluate our model on five more advanced datasets, as shown in Table 5. In particular, our model outperforms the state-of-the-art on CD1 and CD2, by about 18.00% and 13.00% in terms of AUC, and provide pioneering cross-dataset baselines on DFR (99.51%) and DFDC (67.52%). On DFDC-P, our performance is comparable with Face X-ray [25], where we are lower AUC but have a higher AP score, as shown in Table 6. We observe that both our model and state-of-the-art methods cannot achieve appealing results on DFDC/DFDC-P datasets, which motivates us to do more failure analysis in Section 4.6.

The consistency predictions from our model provide interpretable visualization clues about the region of face modification. Qualitative results generated by our cross-dataset models on different datasets are shown in Fig. 5.

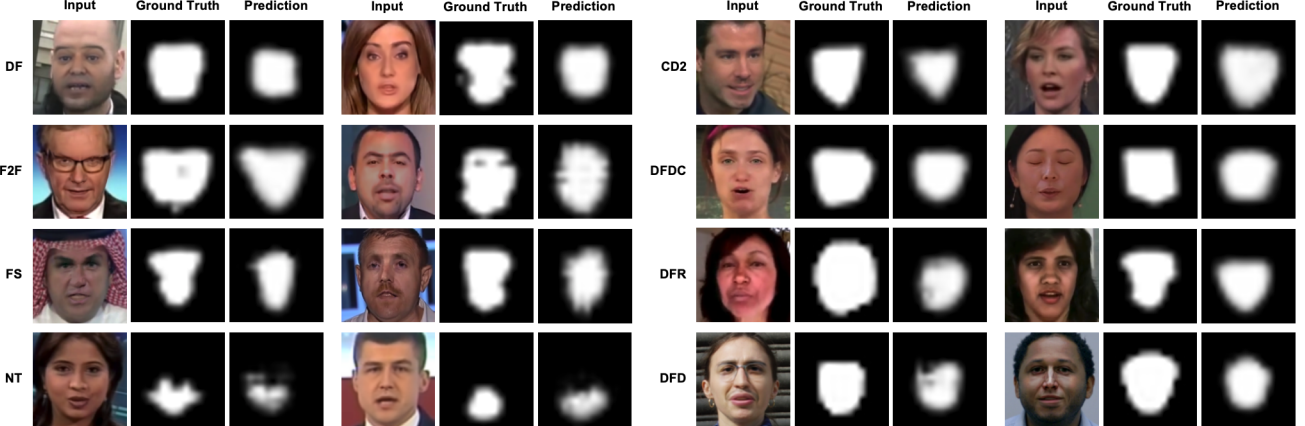


Figure 5: Visualization of the consistency heatmaps, which localize the manipulated regions. The predictions are obtained in the cross-dataset experiments, where our model is trained with only real videos of FF++, augmented by I2G. The ground truth masks are generated by DSSIM, as discussed in Section 4.2.

Method	Backbone	Train Set	Test Set (AUC (%))					
			DF	F2F	FS	NT	FF++	DFD
Face X-ray [25]	HRNet	FF++ (real videos)	99.17	98.57	98.21	<b>98.13</b>	98.52	93.47
PCL + I2G	ResNet-34	FF++ (real videos)	<b>100.00</b>	<b>98.97</b>	<b>99.86</b>	97.63	<b>99.11</b>	<b>99.07</b>

Table 4: Cross-dataset evaluation results on FF++ and DFD. Our model is on par with Face X-ray [25] on FF++, but has better performance on DFD by 5.67% in terms of AUC, with fewer network parameters.

#### 4.5. Ablation Studies

**Effect of PCL.** We impose a weight  $\lambda$  to balance between the consistency and classification losses, as shown in Eq. 4. By setting  $\lambda = 0$ , we disable PCL and get a network architecture equivalent to vanilla ResNet-34 with binary classification loss. To exhibit the advantage of our consistency loss, we train models with increasing  $\lambda$ s and evaluate their cross-dataset generalizations with four test sets. As shown in Table 7, we follow the cross-dataset setting and train all models on real data of FF++ augmented by I2G and report the AUC score for performance comparison. We observe that training with  $\lambda > 0$  significantly outperforms the training with  $\lambda = 0$ . Especially, the performance on DFDC is improved by 15.8% in terms of AUC. The results demonstrate that it is beneficial to use large  $\lambda$  for the training, which also suggests that PCL plays a dominant role in the success.

**Effect of I2G as Joint-Training.** We have been training with our proposed consistency loss on datasets augmented by I2G. I2G generates fake data dynamically during the training, enhancing the training data variety, thereby improving the performance and generalization of our model. To demonstrate the effect of I2G experimentally, we conduct ablation studies by training on either DF or DFDC-P and benchmarking on DFR, CD2, DFDC, and DFDC-P test sets. Results in Table 8 show that models trained on

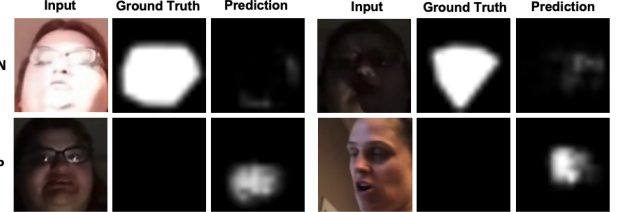


Figure 6: Visualization of false negative (FN) and false positive (FP) predictions on DFDC dataset.

datasets augmented by I2G are able to achieve a significant performance boost. In particular, we train models on the DF with or without I2G, whereas the performance of the latter is improved by an average AUC score of 7.18% over four test sets. The model trained with the DFDC-P train set has noticeably better performance on DFDC and DFDC-P test sets in comparison with the previous models, but generalizes poorly on other datasets such as DFR. I2G significantly improves its generalization, e.g., performance on DFR is raised from 51.61% to 92.25% in terms of AUC, with a minor sacrifice to the performance on DFDC-P.

**Effect of I2G as Pre-Training.** Given a dataset for which even computing the DSSIM masks of Deepfake data is not feasible, one can always use our consistency loss to train a *pretrained model* with any real data augmented by I2G. After that, any standard training for Deepfake detection or related tasks can be conducted with the whole dataset. In particular, we conducted an experiment where we first pre-

Method	Backbone	Train Set	Test Set (AUC (%))				
			DFR	CD1	CD2	DFDC	DFDC-P
Dang <i>et al.</i> [7]	Xception + Reg.	UADFV [61], DFFD [7]	-	71.20	-	-	-
DSP-FWA [29]	ResNet-50	FF++	-	-	69.30	-	-
Xception [45]	Xception	FF++	-	-	73.04	-	-
Masi <i>et al.</i> [33]	LSTM	FF++	-	-	76.65	-	-
Face X-ray [25]	HRNet	FF++	-	80.58	-	-	<b>80.92</b>
PCL + I2G	ResNet-34	FF++ (real data)	<b>99.41</b>	<b>98.30</b>	<b>90.03</b>	<b>67.52</b>	74.37

Table 5: *Cross-dataset evaluation results on DFR, CD1, CD2, DFDC and DFDC-P datasets*. Our model out-performs the state-of-the-arts on CD1 and CD2, by about 18.00% and 13.00% in terms of AUC, and provides pioneering cross-dataset baselines on DFR (99.51%) and DFDC (67.52%). For DFDC-P, we have a lower AUC score but a higher AP score in comparison with the state-of-the-arts (see Table 6).

Method	Backbone	Train Set	Test Set (AP (%))		
			CD1	DFDC-P	
Face X-ray [25]	HRNet	FF++	73.33	72.65	
PCL + I2G	ResNet-34	FF++ (real data)	<b>98.97</b>	<b>82.94</b>	

Table 6: *Cross-dataset evaluation results on CD1 and DFDC-P datasets*. Our models can identify the attack video more precisely.

Method	Hyper-Parameter	Test Set (AUC (%))				Avg
		DFR	CD2	DFDC	DFDC-P	
I2G	$\lambda = 0$	95.12	78.18	51.72	69.93	73.74
PCL + I2G	$\lambda = 1$	99.1	86.52	60.65	74.13	80.10
PCL + I2G	$\lambda = 10$	99.41	90.03	<b>67.52</b>	<b>74.37</b>	<b>82.83</b>
PCL + I2G	$\lambda = 100$	<b>99.78</b>	<b>90.98</b>	63.22	74.36	82.09

Table 7: *Ablation study on the effect of PCL on DFR, CD2, DFDC, and DFDC-P datasets*. The use of large  $\lambda$  significantly improves the cross-dataset performance, especially on DFDC.

Method	Train Set	Test Set (AUC (%))				Avg
		DFR	CD2	DFDC	DFDC-P	
PCL	DF	90.42	84.59	66.26	75.49	79.19
PCL + I2G	DF	<b>99.64</b>	<b>91.92</b>	<b>73.08</b>	<b>80.83</b>	<b>86.37</b>
PCL	DFDC-P	51.61	82.82	69.14	<b>95.53</b>	74.78
PCL + I2G	DFDC-P	<b>92.25</b>	<b>87.65</b>	<b>71.12</b>	94.38	<b>86.35</b>

Table 8: *Ablation study on the effect of I2G as joint-training on DF and DFDC-P datasets*. I2G can enhance the variety of training data, thereby improving the generalization of our model.

trained a ResNet-34 on the real data of DF augmented by I2G for consistency prediction, then finetuned with both real and Deepfake data of DF for classification. We report the evaluation results on DFR, CD2, DFDC, DFDC-P test sets with 99.57%, 91.88%, 68.95%, 79.17% (84.89% on average) in terms of AUC, respectively. These results are unsurprisingly lower than those of joint-training, but they still significantly outperform the baselines. On the other hand, our pretrained models may not necessarily be trained from the established Deepfake datasets. I2G can be potentially applied to any face image or video datasets, such as IMDb-Face [54] and YouTube Faces [60], providing new

and strong pretrained models for Deepfake-related research.

#### 4.6. Failure Cases & Limitations

Although our results are encouraging, our approach has limitations and raise opportunities for future work. First, we only focus on facial image forgeries that are self-inconsistent. It is unknown whether it is applicable to entire face synthesis, where the consistency is supposed to be high across all regions. Second, we investigate the failure cases in DFDC, as shown in Fig. 6. From false negative samples, we observed that the quality of the samples is low in the dataset due to the high compression, high/low exposure that some of the samples cannot be recognized. Therefore, the cost of Deepfake generation is highly increased to bypass our system. From false positive samples, we observed the inconsistency is caught by our model in some cases, which might be caused by the lighting and unusual texture.

## 5. Conclusion

In this paper, we proposed to use patch-wise consistency learning for detecting face manipulations and localizing the Deepfake forged regions. To provide the pixel-level annotations, Inconsistency Image Generator (I2G) is developed to generate “self-inconsistent” images from the pristine ones. The designed consistency comparison module only requires minor modification upon the standard backbones and provides a visual explanation of face manipulation without extra deconvolutions. We demonstrate that our method has superior generalization ability, since the classification based on consistency features instead of forgery features is more generalizable to unseen generation techniques. Our model can also be adopted as pretrained initialization for downstream datasets from which the consistency labels are not available. On the other hand, the proposed I2G pipeline is also effective in improving the cross-domain generalization of our models. Extensive experiments are conducted to exhibit that our approach is competitive in comparison with the state-of-the-art on seven widely used datasets, providing strong baselines for future research.

## References

[1] Darius Afchar, Vincent Nozick, Junichi Yamagishi, and Isao Echizen. Mesonet: a compact facial video forgery detection network. In *Proc. Workshop on Information Forensics and Security*, 2018. 12

[2] Edoardo Ardizzone, Alessandro Bruno, and Giuseppe Mazzola. Copy-move forgery detection by matching triangles of keypoints. *IEEE Transactions on Information Forensics and Security*, 10(10):2084–2094, 2015. 1

[3] Mauro Barni, Luca Bondi, Nicolo Bonettini, Paolo Bestagini, Andrea Costanzo, Marco Maggini, Benedetta Tondi, and Stefano Tubaro. Aligned and non-aligned double jpeg detection using convolutional neural networks. *Journal of Visual Communication and Image Representation*, 49:153–163, 2017. 1

[4] Luca Bondi, Luca Baroffio, David Güera, Paolo Bestagini, Edward J Delp, and Stefano Tubaro. First steps toward camera model identification with convolutional neural networks. *IEEE Signal Processing Letters*, 24(3):259–263, 2016. 2

[5] Adrian Bulat and Georgios Tzimiropoulos. How far are we from solving the 2D & 3D face alignment problem? (and a dataset of 230,000 3D facial landmarks). In *Proc. IEEE/CVF International Conference on Computer Vision*, pages 1021–1030, Oct. 22–29 2017. 5

[6] Yunjey Choi, Youngjung Uh, Jaejun Yoo, and Jung-Woo Ha. StarGAN v2: Diverse image synthesis for multiple domains. In *Proc. IEEE/CVF Conference on Computer Vision and Pattern Recognition*, pages 8188–8197, Jun. 14–19 2020. 2

[7] Hao Dang, Feng Liu, Joel Stehouwer, Xiaoming Liu, and Anil Jain. On the detection of digital face manipulation. In *Proc. IEEE/CVF Conference on Computer Vision and Pattern Recognition*, pages 5781–5790, Jun. 14–19 2020. 1, 2, 8

[8] Oscar de Lima, Sean Franklin, Shreshtha Basu, Blake Karwoski, and Annet George. Deepfake detection using spatiotemporal convolutional networks. *arXiv:2006.14749*, 2020. 1, 2

[9] Jia Deng, Wei Dong, Richard Socher, Li-Jia Li, Kai Li, and Li Fei-Fei. ImageNet: A large-scale hierarchical image database. In *Proc. IEEE/CVF Conference on Computer Vision and Pattern Recognition*, pages 248–255, Jun. 20–25 2009. 5

[10] Brian Dolhansky, Joanna Bitton, Ben Pflaum, Jikuo Lu, Russ Howes, Menglin Wang, and Cristian Canton Ferrer. The deepfake detection challenge dataset. *arXiv:2006.07397*, 2020. 2, 4, 5, 12

[11] Brian Dolhansky, Russ Howes, Ben Pflaum, Nicole Baram, and Cristian Canton Ferrer. The deepfake detection challenge (dfdc) preview dataset. *arXiv:1910.08854*, 2019. 5, 12

[12] Nick Dufour and Andrew Gully. Contributing data to deepfake detection research, 2019. <https://ai.googleblog.com/2019/09/contributing-data-to-deepfake-detection.html>. 2, 5, 12

[13] FaceSwapDevs. Deepfakes, 2019. <https://github.com/deepfakes/faceswap>. 5, 12

[14] Chistian Conton Ferrer, Brian Colhansky, Ben Pflaum, Joanna Bitton, Jacqueline Pan, and Jikuo Lu. Deepfake detection challenge results: An open initiative to advance ai, 2020. <https://ai.facebook.com/blog/deepfake-detection-challenge-results-an-open-initiative-to-advance-ai/>. 6

[15] Kaiming He, Xiangyu Zhang, Shaoqing Ren, and Jian Sun. Deep Residual Learning for Image Recognition. In *Proc. IEEE/CVF Conference on Computer Vision and Pattern Recognition*, pages 770–778, Jun. 26–Jul. 1 2016. 5

[16] Yihao Huang, Felix Juefei-Xu, Run Wang, Xiaofei Xie, Lei Ma, Jianwen Li, Weikai Miao, Yang Liu, and Geguang Pu. FakeLocator: Robust localization of GAN-based face manipulations via semantic segmentation networks with bells and whistles. *arXiv:2001.09598*, 2020. 2

[17] Minyoung Huh, Andrew Liu, Andrew Owens, and Alexei A. Efros. Fighting fake news: Image splice detection via learned self-consistency. In *Proc. European Conference on Computer Vision*, pages 101–117, Sep 8–14 2018. 1, 2

[18] Liming Jiang, Ren Li, Wayne Wu, Chen Qian, and Chen Change Loy. DeeperForensics-1.0: A large-scale dataset for real-world face forgery detection. In *Proc. IEEE/CVF Conference on Computer Vision and Pattern Recognition*, pages 2886–2895, Jun. 14–19 2020. 2, 5, 12

[19] Tero Karras, Samuli Laine, and Timo Aila. A style-based generator architecture for generative adversarial networks. In *Proc. IEEE/CVF Conference on Computer Vision and Pattern Recognition*, pages 4401–4410, Jun. 16–20 2019. 2

[20] Tero Karras, Samuli Laine, Miika Aittala, Janne Hellsten, Jaakko Lehtinen, and Timo Aila. Analyzing and improving the image quality of StyleGAN. *arXiv:1912.04958*, 2019. 2

[21] Diederik P. Kingma and Jimmy Ba. Adam: A method for stochastic optimization. In *Proc. International Conference on Learning Representations*, 2015. 5

[22] Pavel Korshunov and Sébastien Marcel. DeepFakes: a new threat to face recognition? assessment and detection. *arXiv:1812.08685*, 2018. 2

[23] Marek Kowalski. FaceSwap, 2018. <https://github.com/MarekKowalski/FaceSwap>. 5, 12

[24] Akash Kumar and Arnav Bhavsar. Detecting deepfakes with metric learning. *arXiv:2003.08645*, 2020. 1, 2

[25] Lingzhi Li, Jianmin Bao, Ting Zhang, Hao Yang, Dong Chen, Fang Wen, and Baining Guo. Face X-ray for more general face forgery detection. In *Proc. IEEE/CVF Conference on Computer Vision and Pattern Recognition*, pages 5001–5010, Jun. 14–19 2020. 1, 2, 4, 5, 6, 7, 8

[26] Wei Li, Yuanjun Xiong, Shuo Yang, Siqi Deng, and Wei Xia. SMOT: Single-shot multi object tracking. *arXiv:2010.16031*, 2020. 5

[27] Xiaodan Li, Yining Lang, Yuefeng Chen, Xiaofeng Mao, Yuan He, Shuhui Wang, Hui Xue, and Quan Lu. Sharp multiple instance learning for DeepFake video detection. In *Proc. ACM Multimedia*, Oct. 12–16 2020. 6

[28] Yuezun Li, Ming-Ching Chang, and Siwei Lyu. In ictu oculi: Exposing ai created fake videos by detecting eye blinking. In *Proc. International Workshop on Information Forensics and Security*, 2018. 1

[29] Yuezun Li and Siwei Lyu. Exposing deepfake videos by detecting face warping artifacts. In *Proc. IEEE/CVF Conference on Computer Vision and Pattern Recognition Work-*

shops, Jun. 16–20 2019. 1, 2, 4, 8, 12

[30] Yuezun Li, Xin Yang, Pu Sun, Honggang Qi, and Siwei Lyu. Celeb-DF: A large-scale challenging dataset for deepfake forensics. In *Proc. IEEE/CVF Conference on Computer Vision and Pattern Recognition*, pages 3207–3216, Jun. 14–19 2020. 2, 5, 12

[31] Ming Liu, Yukang Ding, Min Xia, Xiao Liu, Errui Ding, Wangmeng Zuo, and Shilei Wen. STGAN: A unified selective transfer network for arbitrary image attribute editing. In *Proc. IEEE/CVF Conference on Computer Vision and Pattern Recognition*, pages 3673–3682, Jun. 16–20 2019. 2

[32] Jan Lukas, Jessica Fridrich, and Miroslav Goljan. Determining digital image origin using sensor imperfections. In *Proc. Image and Video Communications and Processing*, 2005. 1

[33] Iacopo Masi, Aditya Killekar, Royston Marian Mascarenhas, Shenoy Pratik Gurudatt, and Wael AbdAlmageed. Two-branch recurrent network for isolating deepfakes in videos. In *Proc. European Conference on Computer Vision*, Aug. 23–28 2020. 6, 8, 12

[34] Falko Matern, Christian Riess, and Marc Stamminger. Exploiting visual artifacts to expose deepfakes and face manipulations. In *Proc. Winter Applications of Computer Vision Workshops*, 2019. 12

[35] Owen Mayer and Matthew C Stamm. Learned forensic source similarity for unknown camera models. In *International Conference on Acoustics, Speech and Signal Processing*, pages 2012–2016, 2018. 2

[36] Owen Mayer and Matthew C Stamm. Forensic similarity for digital images. *IEEE Transactions on Information Forensics and Security*, 15:1331–1346, 2019. 2

[37] Owen Mayer and Matthew C Stamm. Exposing fake images with forensic similarity graphs. *IEEE Journal of Selected Topics in Signal Processing*, 14(5):1049–1064, 2020. 2

[38] Jacek Naruniec, Leonhard Helminger, Christopher Schroers, and Romann M. Weber. High-resolution neural face swapping for visual effects. In *Proc. Eurographics Symposium on Rendering*, 2020. 4

[39] João C. Neves, Ruben Tolosana, Ruben Vera-Rodriguez, Vasco Lopes, Hugo Proença, and Julian Fierrez. GANprintR: Improved fakes and evaluation of the state-of-the-art in face manipulation detection. *Journal of Selected Topics in Signal Processing*, 14(5):1038–1048, 2020. 2

[40] Huy H. Nguyen, Fuming Fang, Junichi Yamagishi, and Isao Echizen. Multi-task learning for detecting and segmenting manipulated facial images and videos. In *Proc. Biometrics Theory, Applications and Systems*, Sep. 23–26 2019. 1, 2, 12

[41] Huy H Nguyen, Junichi Yamagishi, and Isao Echizen. Capsule-forensics: Using capsule networks to detect forged images and videos. In *Proc. International Conference on Acoustics, Speech and Signal Processing*, 2019. 12

[42] Patrick Pérez, Michel Gangnet, and Andrew Blake. Poisson image editing. *ACM Transactions on Graphics*, 2003. 4

[43] Ivan Perov, Daiheng Gao, Nikolay Chervonyi, Kunlin Liu, Sugasa Marangonda, Chris Umé, Mr. Dpfks, Carl Shift Facenheim, Luis RP, Jian Jiang, Sheng Zhang, Pingyu Wu, Bo Zhou, and Weiming Zhang. DeepFaceLab: A simple, flexible and extensible face swapping framework. *arXiv:2005.05535*, 2020. 1

[44] Olaf Ronneberger, Philipp Fischer, and Thomas Brox. U-Net: Convolutional networks for biomedical image segmentation. In *Proc. Medical Image Computing and Computer-assisted Intervention*, 2015. 4

[45] Andreas Rössler, Davide Cozzolino, Luisa Verdoliva, Christian Riess, Justus Thies, and Matthias Nießner. FaceForensics++: Learning to detect manipulated facial images. In *Proc. IEEE/CVF International Conference on Computer Vision*, pages 1–11, Oct. 27–Nov. 2 2019. 2, 5, 6, 8, 12

[46] Ekraam Sabir, Jiaxin Cheng, Ayush Jaiswal, Wael AbdAlmageed, Iacopo Masi, and Prem Natarajan. Recurrent convolutional strategies for face manipulation detection in videos. In *Proc. IEEE/CVF Conference on Computer Vision and Pattern Recognition Workshop*, Jun. 16–20 2019. 2

[47] Ayush Tewari, Michael Zollhofer, Hyeongwoo Kim, Pablo Garrido, Florian Bernard, Patrick Perez, and Christian Theobalt. MoFA: Model-based deep convolutional face autoencoder for unsupervised monocular reconstruction. In *Proc. IEEE/CVF International Conference on Computer Vision Workshops*, pages 1274–1283, Oct. 22–29 2017. 2

[48] J. Thies, M. Zollhöfer, M. Stamminger, C. Theobalt, and M. Nießner. Face2Face: Real-time Face Capture and Reenactment of RGB Videos. In *Proc. IEEE/CVF Conference on Computer Vision and Pattern Recognition*, pages 2387–2395, Jun. 26–Jul. 1 2016. 2, 5, 12

[49] Justus Thies, Michael Zollhöfer, and Matthias Nießner. Deferred neural rendering: Image synthesis using neural textures. In *ACM Transactions on Graphics*, volume 38, pages 1–12, 2019. 5, 12

[50] Ruben Tolosana, Sergio Romero-Tapiador, Julian Fierrez, and Ruben Vera-Rodriguez. DeepFakes evolution: Analysis of facial regions and fake detection performance. *arXiv:2004.07532*, 2020. 1, 2, 6

[51] Ruben Tolosana, Ruben Vera-Rodriguez, Julian Fierrez, Aythami Morales, and Javier Ortega-Garcia. Deepfakes and beyond: A survey of face manipulation and fake detection. *arXiv preprint arXiv:2001.00179*, 2020. 2

[52] Loc Trinh, Michael Tsang, Sirisha Rambhatla, and Yan Liu. Interpretable deepfake detection via dynamic prototypes. *arXiv:2006.15473*, 2020. 1

[53] Arash Vahdat and Jan Kautz. NVAE: A deep hierarchical variational autoencoder. In *Proc. Advances in Neural Information Processing Systems*, Dec. 6–12 2020. 2

[54] Fei Wang, Liren Chen, Cheng Li, Shiyao Huang, Yanjie Chen, Chen Qian, and Chen Change Loy. The devil of face recognition is in the noise. *arXiv:1807.11649*, 2018. 8

[55] Run Wang, Felix Juefei-Xu, Lei Ma, Xiaofei Xie, Yihao Huang, Jian Wang, and Yang Liu. FakeSpotter: A simple yet robust baseline for spotting ai-synthesized fake faces. *arXiv:1909.06122*, 2019. 1, 2, 6

[56] Sheng-Yu Wang, Oliver Wang, Richard Zhang, Andrew Owens, and Alexei A. Efros. CNN-generated images are surprisingly easy to spot... for now. In *Proc. IEEE/CVF Conference on Computer Vision and Pattern Recognition*, pages 8695–8704, Jun 14–19 2020. 2

[57] Xiaolong Wang, Ross Girshick, Abhinav Gupta, and Kaiming He. Non-local neural networks. In *Proc. IEEE/CVF Conference on Computer Vision and Pattern Recognition*, pages 7794–7803, Jun. 18–22 2018. 3

[58] Xinggang Wang, Yongluan Yan, Peng Tang, Xiang Bai, and

Wenyu Liu. Revisiting multiple instance neural networks. *Pattern Recognition*, 74:15–24, 2018. 6

[59] Zhou Wang, Alan C Bovik, Hamid R Sheikh, and Eero P Simoncelli. Image quality assessment: from error visibility to structural similarity. *IEEE Transactions on Image Processing*, 13(4):600–612, 2004. 5

[60] Lior Wolf, Tal Hassner, and Itay Maoz. Face recognition in unconstrained videos with matched background similarity. In *Proc. IEEE/CVF Conference on Computer Vision and Pattern Recognition*, pages 529–534, Jun. 20–25 2011. 8

[61] Xin Yang, Yuezun Li, and Siwei Lyu. Exposing deep fakes using inconsistent head poses. In *International Conference on Acoustics, Speech, and Signal Processing*, 2018. 2, 8, 12

[62] Ning Yu, Larry Davis, and Mario Fritz. Attributing fake images to GANs: Analyzing fingerprints in generated images. In *Proc. IEEE/CVF International Conference on Computer Vision*, pages 7556–7566, Oct. 27–Nov. 2 2019. 1, 2

[63] P. Zhou, X. Han, V. I. Morariu, and L. S. Davis. Two-stream neural networks for tampered face detection. In *Proc. IEEE/CVF Conference on Computer Vision and Pattern Recognition Workshops*, Jun. 21–26 2017. 1, 2, 12

[64] Bojia Zi, Minghao Chang, Jingjing Chen, Xingjun Ma, and Yu-Gang Jiang. WildDeepfake: A challenging real-world dataset for deepfake detection. In *Proc. ACM International Conference on Multimedia*, pages 2382–2390, Oct. 2020. 2

## A. Video-Level Comprehensive Results

To provide a comprehensive benchmark for future work on Deepfake detection, we report the performance of our model on seven popular datasets in terms of AUC, AP, and EER. The results are shown in Table 9. Note that the evaluation results are at *video-level*, computed by averaging the classification scores of the video frames. All of these experiments are conducted under the *cross-dataset* setting, where we train our model with only real videos from the raw version of FF++ [45] and the fake/positive samples are generated by I2G (see Sec. 4.2 for more details).

**Additional qualitative results** are shown in Fig. 7. These images are randomly chosen from Celeb-DF-v2 [30] and DFDC Public test set [10], which are among the most challenging datasets in Deepfake detection. In particular, we visualize the consistency maps from true positive, false negative, true negative, and false positive predictions to help fully interpret our model.

Method	Test Set	Evaluation Metrics (%)		
		AUC	AP	EER
PCL + I2G	DF [13]	100.00	100.00	0.00
	F2F [48]	98.97	99.32	3.57
	FS [23]	99.86	99.86	1.43
	NT [49]	97.63	98.20	6.43
	FF++ [45]	99.11	99.80	3.57
	DFD [12]	99.07	99.89	4.42
	DFR [18]	99.41	99.51	3.48
	CD1 [30]	98.30	98.97	7.89
	CD2 [30]	90.03	94.45	17.98
	DFDC [10]	67.52	69.99	37.18
	DFDC-P [11]	74.37	82.94	31.87

Table 9: Comprehensive evaluation of our model in terms of video-level AUC, AP, and EER on seven datasets.

## B. Frame-Level Results on Celeb-DF-v2

Besides the video-level evaluation, we also compare our model with state-of-the-art methods in terms of frame-level AUC on CD2 [30], where our model is trained under the *cross-dataset* setting (see Sec. 4.2 for more details). As shown in Table 10, our model outperforms the state-of-the-art method [33] by over 8%.

Method	CD2 (Frame-Level AUC (%))
Two-stream [63]	53.8
Meso4 [1]	54.8
MesoInception4	53.6
HeadPose [61]	54.6
FWA [29]	56.9
VA-MLP [34]	55.0
VA-LogReg	55.1
Xception-raw [45]	48.2
Xception-c23	65.3
Xception-c40	65.5
Multi-task [40]	54.3
Capsule [41]	57.5
DSP-FWA [29]	64.6
Masi <i>et al.</i> [33]	73.4
PCL + I2G	<b>81.8</b>

Table 10: Cross-dataset evaluation results of our model in terms of frame-level AUC on CD2 dataset. The performance of existing methods are cited for comparison.

## C. Test Set Statistics

Test Set	# Real / Fake Videos
FaceForensics++ (FF++) [45]	140 / 560
FF++ - Deepfakes (DF) [13]	140 / 140
FF++ - Face2Face (F2F) [48]	140 / 140
FF++ - FaceSwap (FS) [23]	140 / 140
FF++ - NeuralTextures (NT) [49]	140 / 140
DeepfakeDetection (DFD) [12]	363 / 3431
Celeb-DF-v1 (CD1) [30]	38 / 62
Celeb-DF-v2 (CD2) [30]	178 / 340
DFDC Public (DFDC) [10]	2000 / 2000
DFDC Preview (DFDC-P) [11]	276 / 504
DeeperForensics-1.0 (DFR) [18]	201 / 201

Table 11: Statistics of real and fake videos in the test sets.

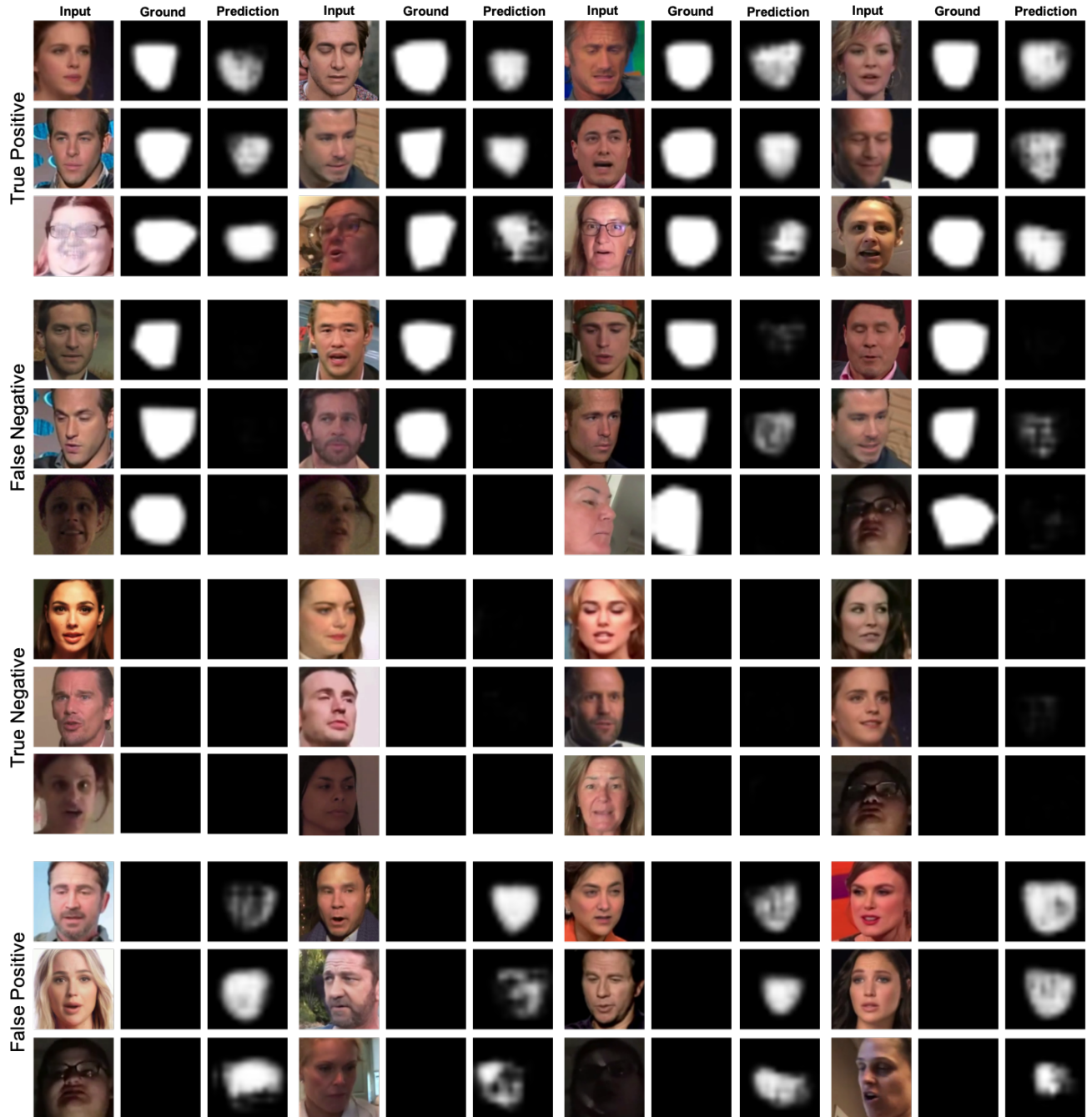


Figure 7: *Visualization of the consistency maps, which localize the manipulated regions.* The predictions are obtained in the cross-dataset experiments, where our model is trained with only real videos of FF++, augmented by I2G. The ground truth masks are generated by DSSIM, as discussed in Section 4.2.